ON THE NATURE AND CONTENT OF QUASAR JETS

Marek Sikora

Copernicus Astronomical Center, Warsaw

SLAC, 28 APRIL, 2005

T

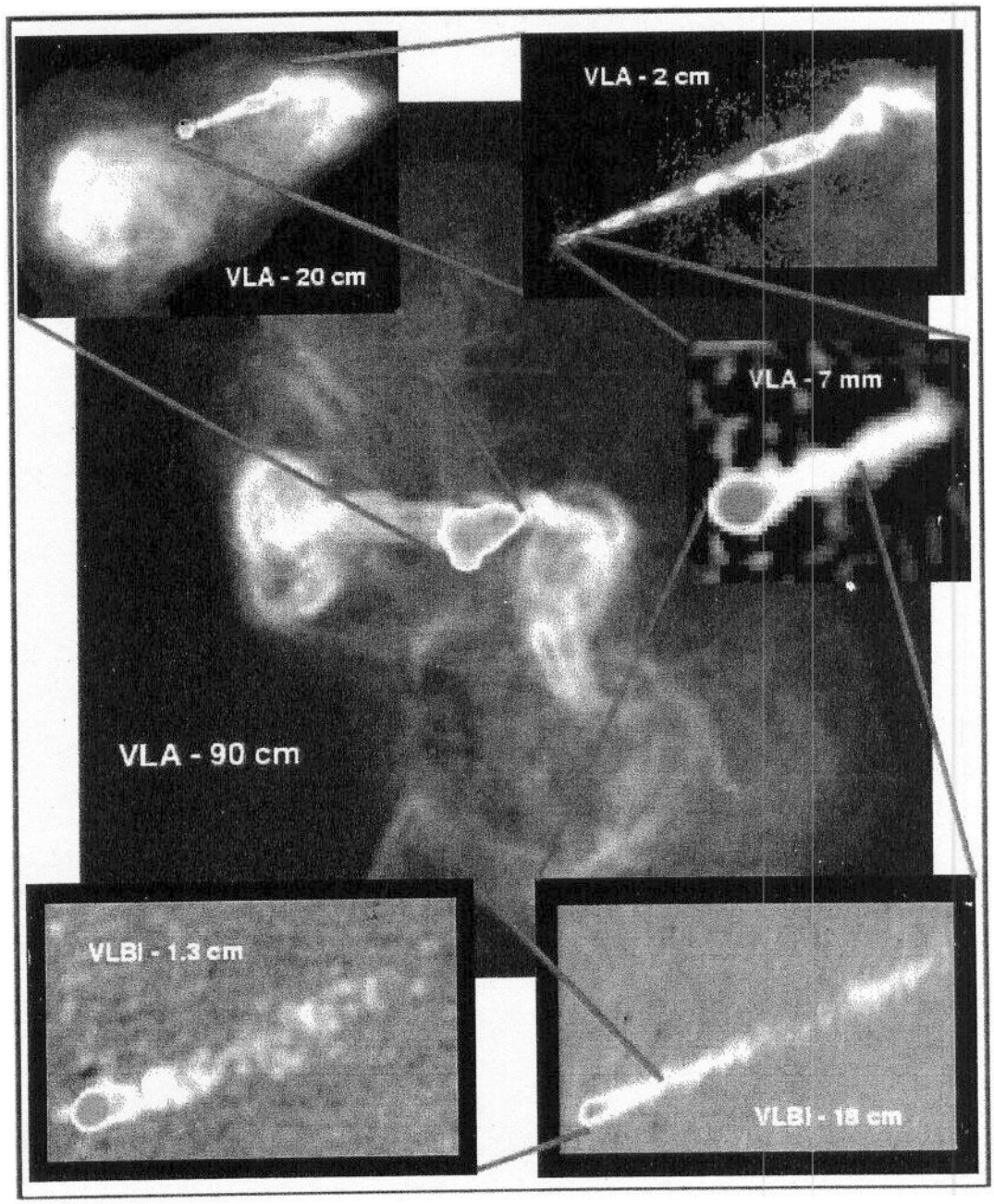

Top page The Inner Lobes

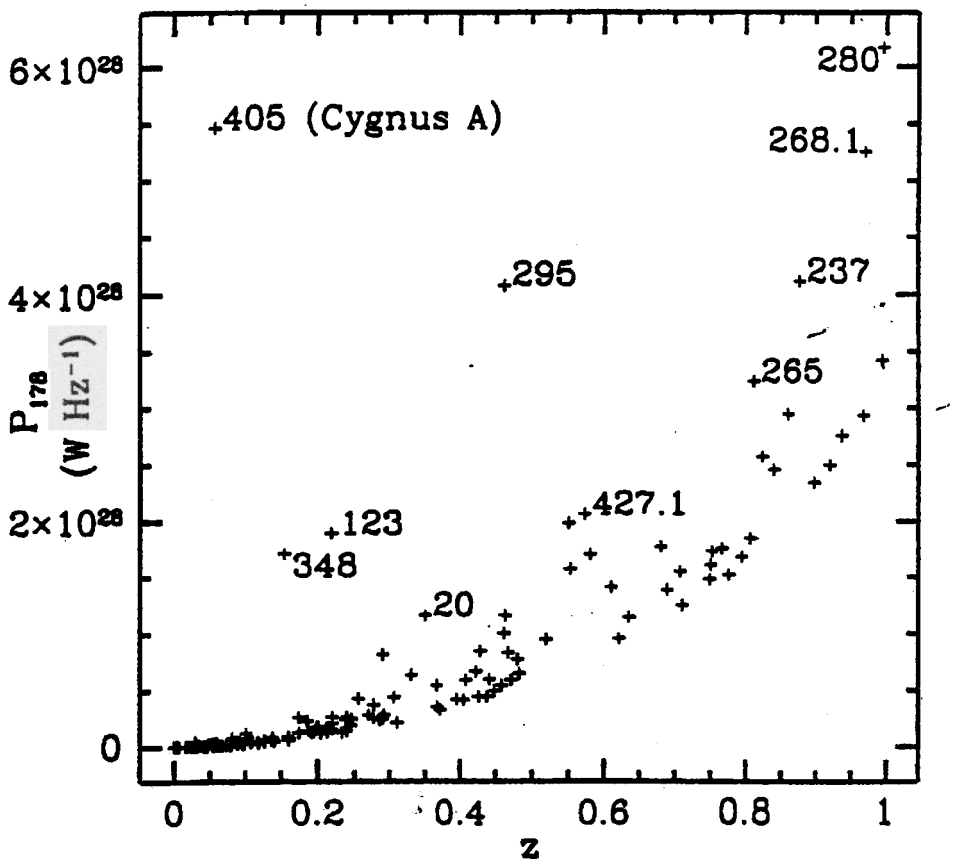

Fig. 1. The radio power–redshift relation for the 3C sample of $z < 1$ FRII radio galaxies, calculated using $H_0 = 75$ km sec^{-1}Mpc^{-1} and $q_0 = 0.5$ (from Stockton and Ridgeway 1996). The more luminous sources are labeled

Cygnus A at 5 GHz

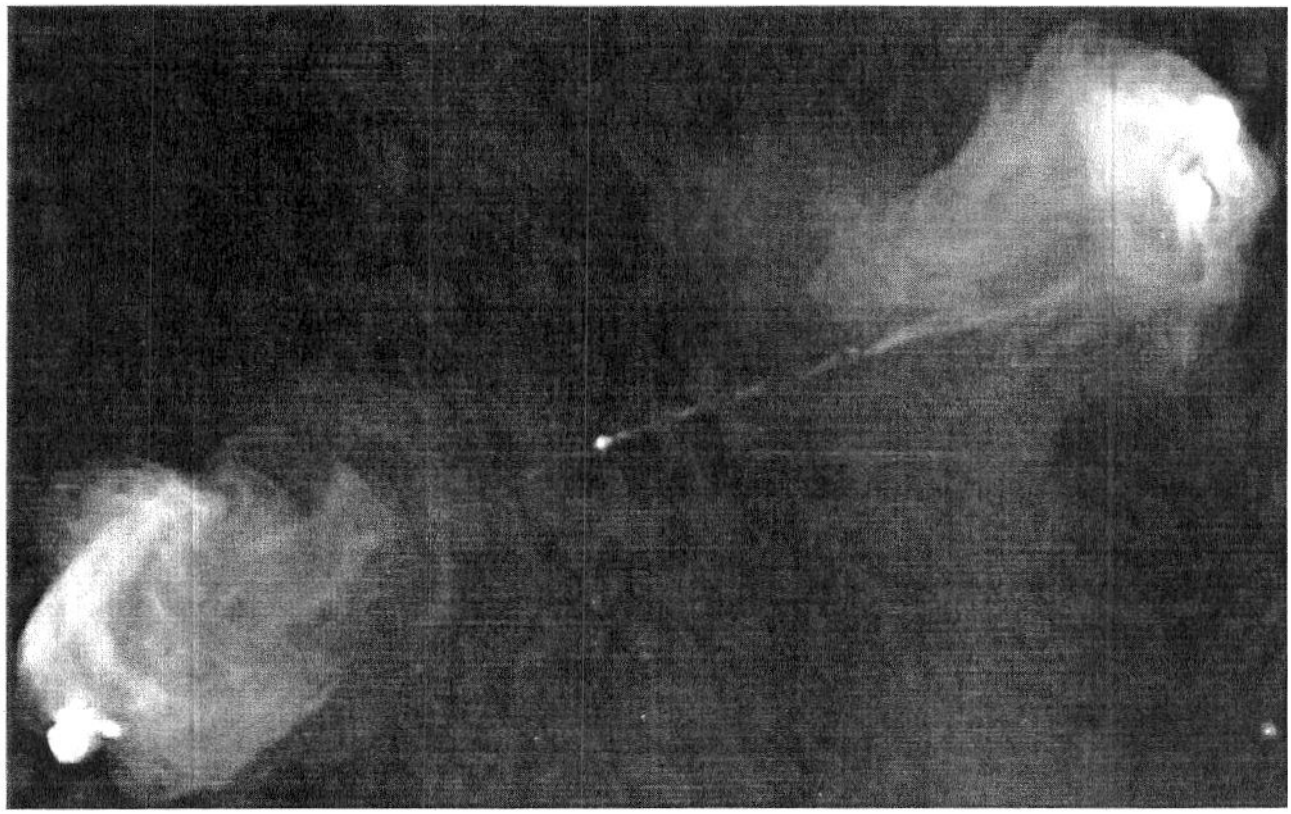

The radio galaxy Cygnus A as seen by the Very Large Array at 5 GHz, 0.5'' resolution. The galaxy is at a redshift of 0.057 (distance = 230 Mpc = 760 ly). See Carilli and Barthel 1996, A&A Reviews, 7, 1 for details.

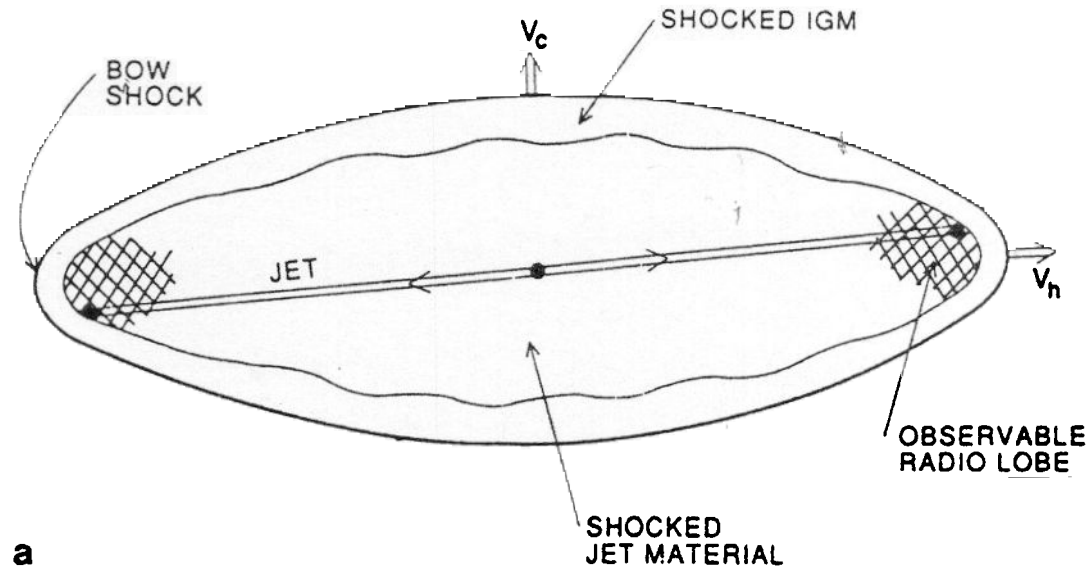

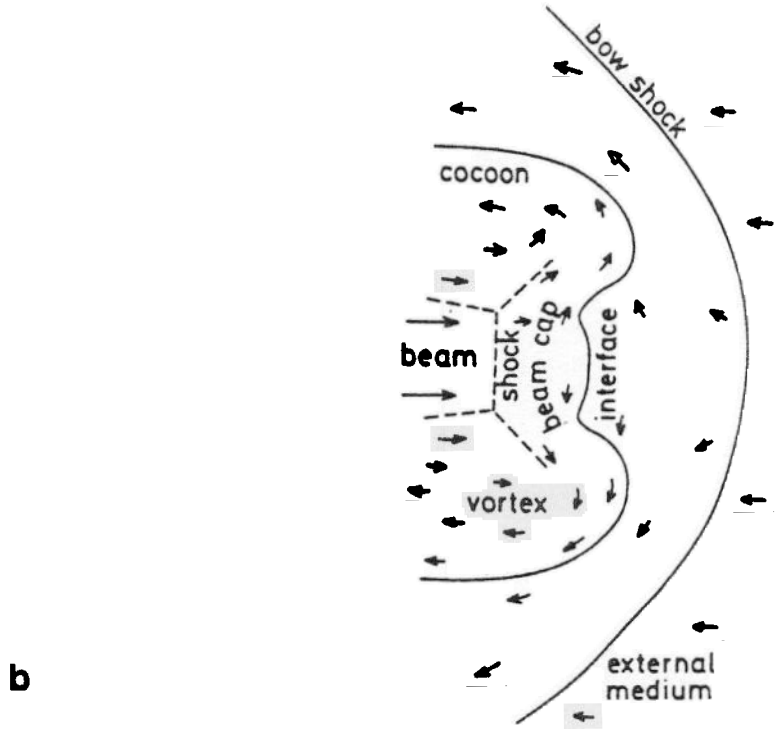

Fig. 3A,B. A schematic representation showing the effect an expanding radio source will have on the external medium. Fig. A is reproduced from Begelman and Cioffi (1989), and shows the expected large-scale distribution of shocked ambient gas enveloping the radio lobes. Figure B is reproduced from Smith et al. (1985) and shows a detail of the expected double-shock structure at the jet terminus. The interface is the contact discontinuity between shocked jet material and shocked intracluster material (ICM). The beam shock and cap correspond to the radio hotspots, and the cocoon corresponds to the radio lobe

Morphology, onesidness, and double hot spots

⇓

Large scale jets are relativistic and light — $\rho_j' < \rho_{IGM}(r^2$

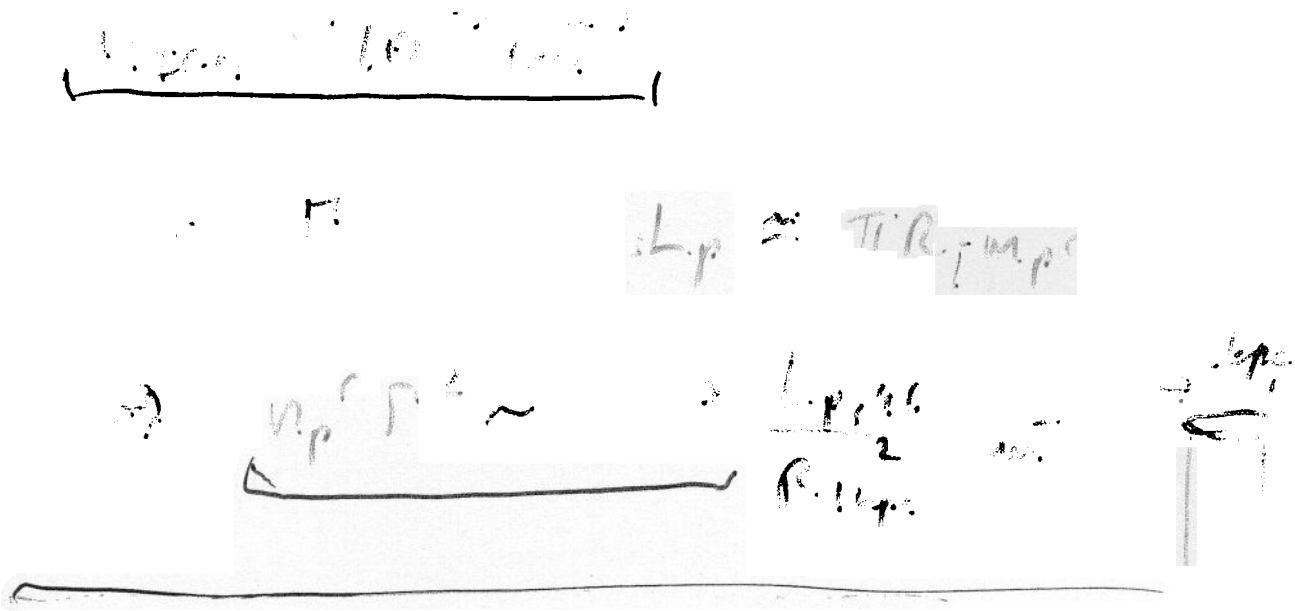

Baby double radio-sources (CSS, GHP)

⇓

jets may be light down to parsec distances

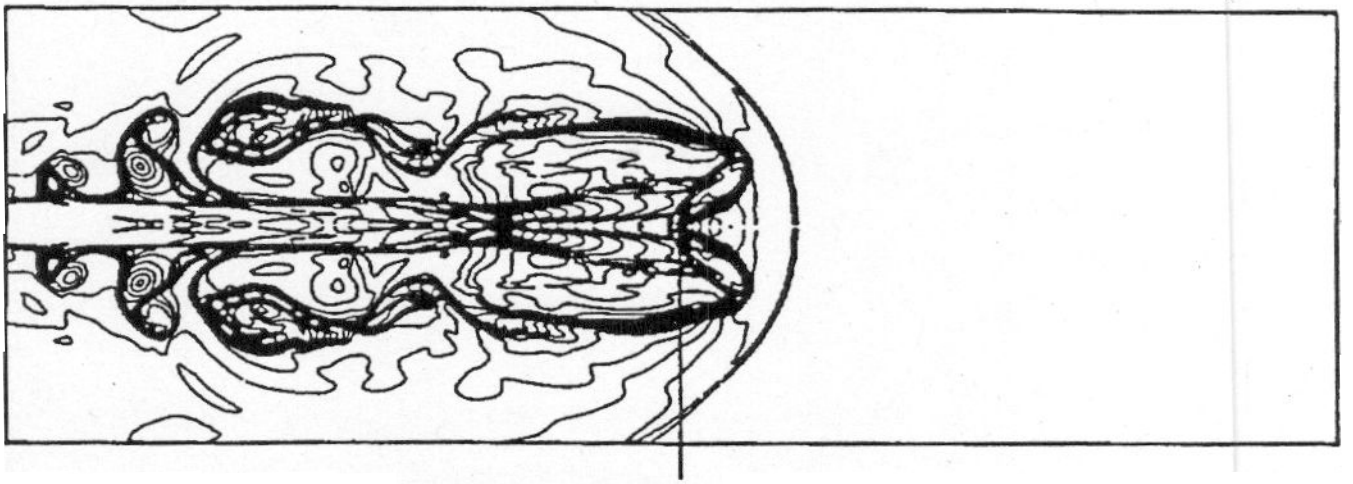
Terminal Mach Disk

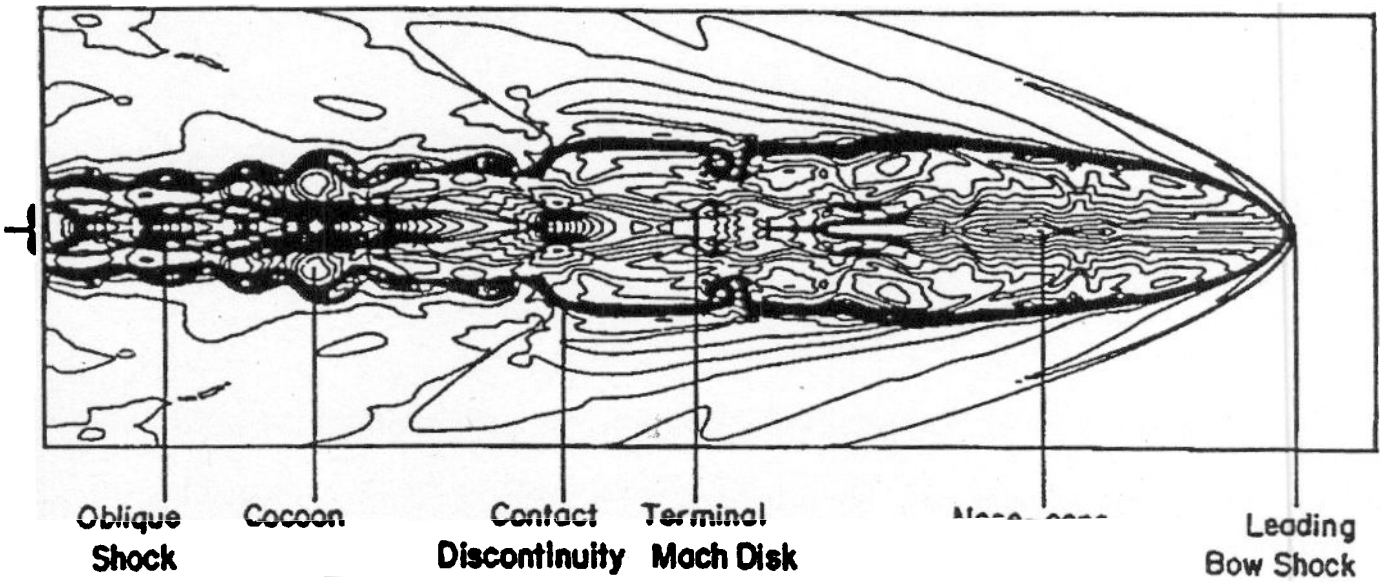
Oblique Shock
Cocoon
Contact Discontinuity
Terminal Mach Disk
Leading Bow Shock

Numerical simulations by

[illegible]

[illegible]

[illegible]

Magnetically dominated jets do not develop substantial back-flowing cocoons. Instead the shocked jet plasma, being confined by magnetic stresses, forms a "nose-cone"-shaped heads.

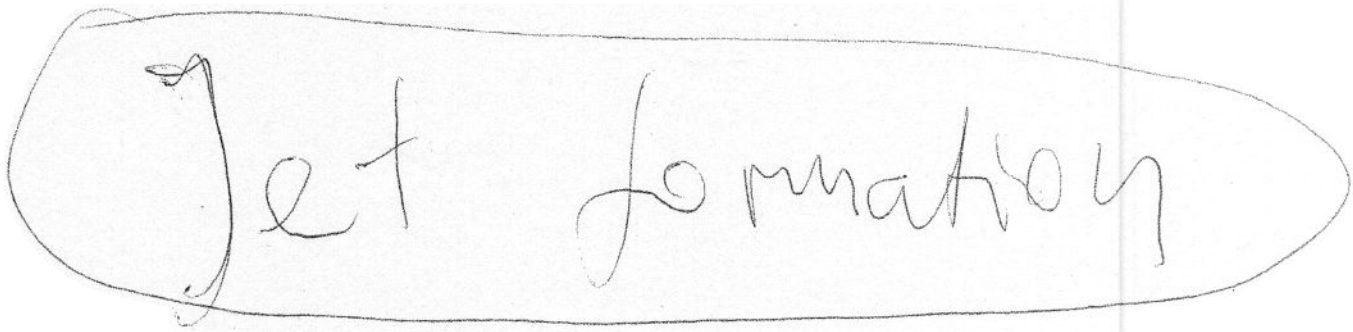
Jet formation

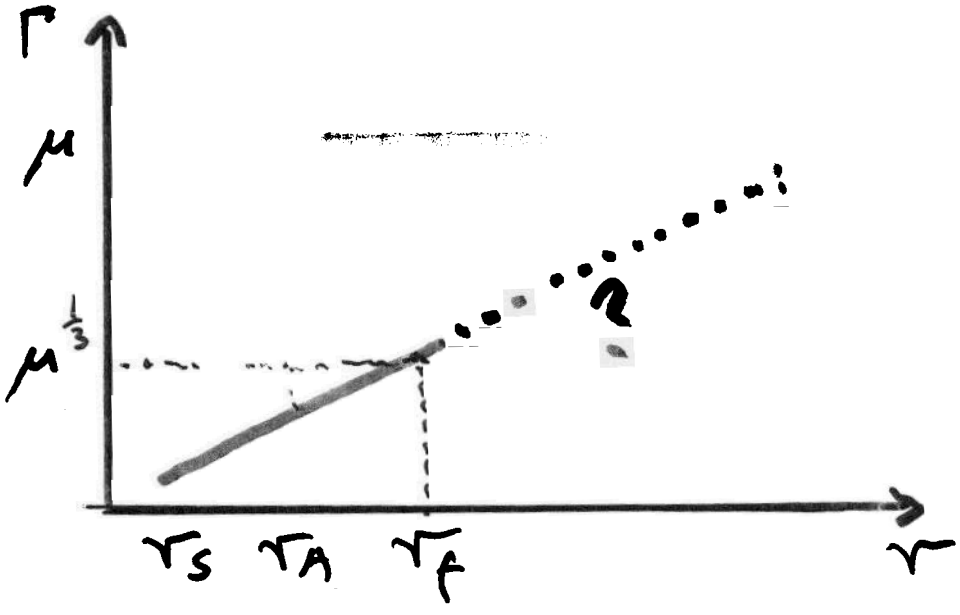

$$\mu = \frac{L_j}{\dot{M}_j c^2} \qquad L_j = L_B + L_K \simeq L_{B_0}$$

where $L_B = \pi R_j^2 \frac{B_\varphi^2}{4\pi} c$

$$L_K = \dot{M}_j c^2 (\Gamma - 1)$$

$$\sigma = \frac{L_B}{L_K}$$

Poynting jets : $\sigma \gg 1$

Kinetic jets : $\sigma \ll 1$ $(\Gamma \sim \mu)$

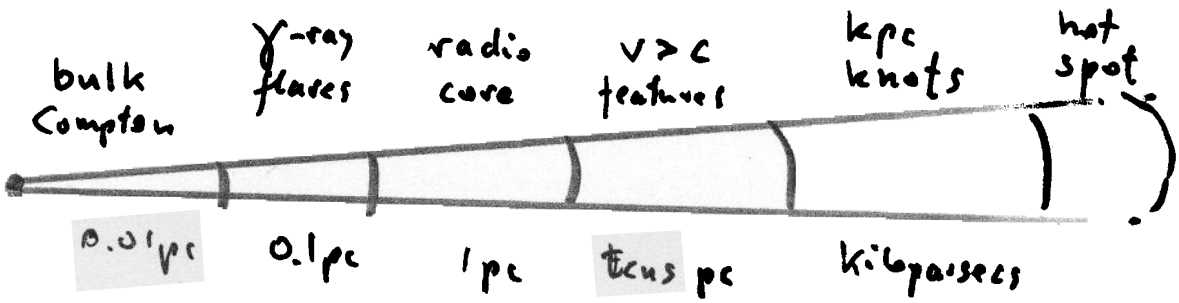
bulk Compton
γ-ray flares
radio core
v > c features
kpc knots
hot spot
0.01 pc
0.1 pc
1 pc
tens pc
kiloparsecs

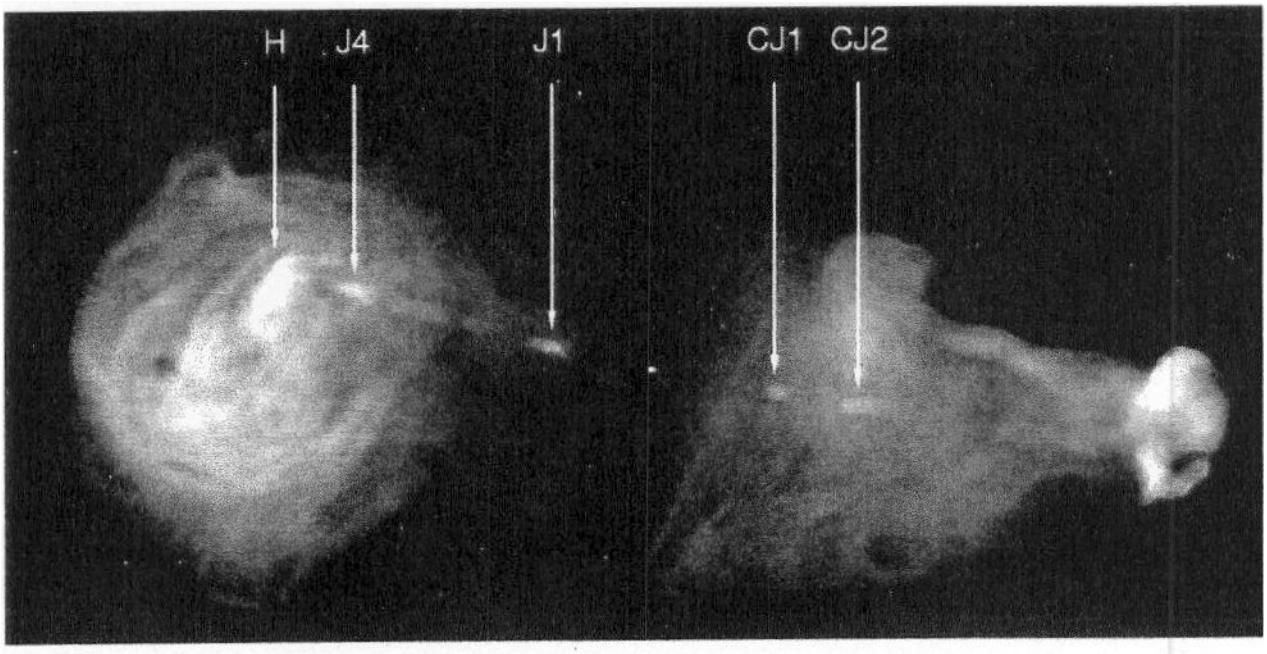

Swain et al '98

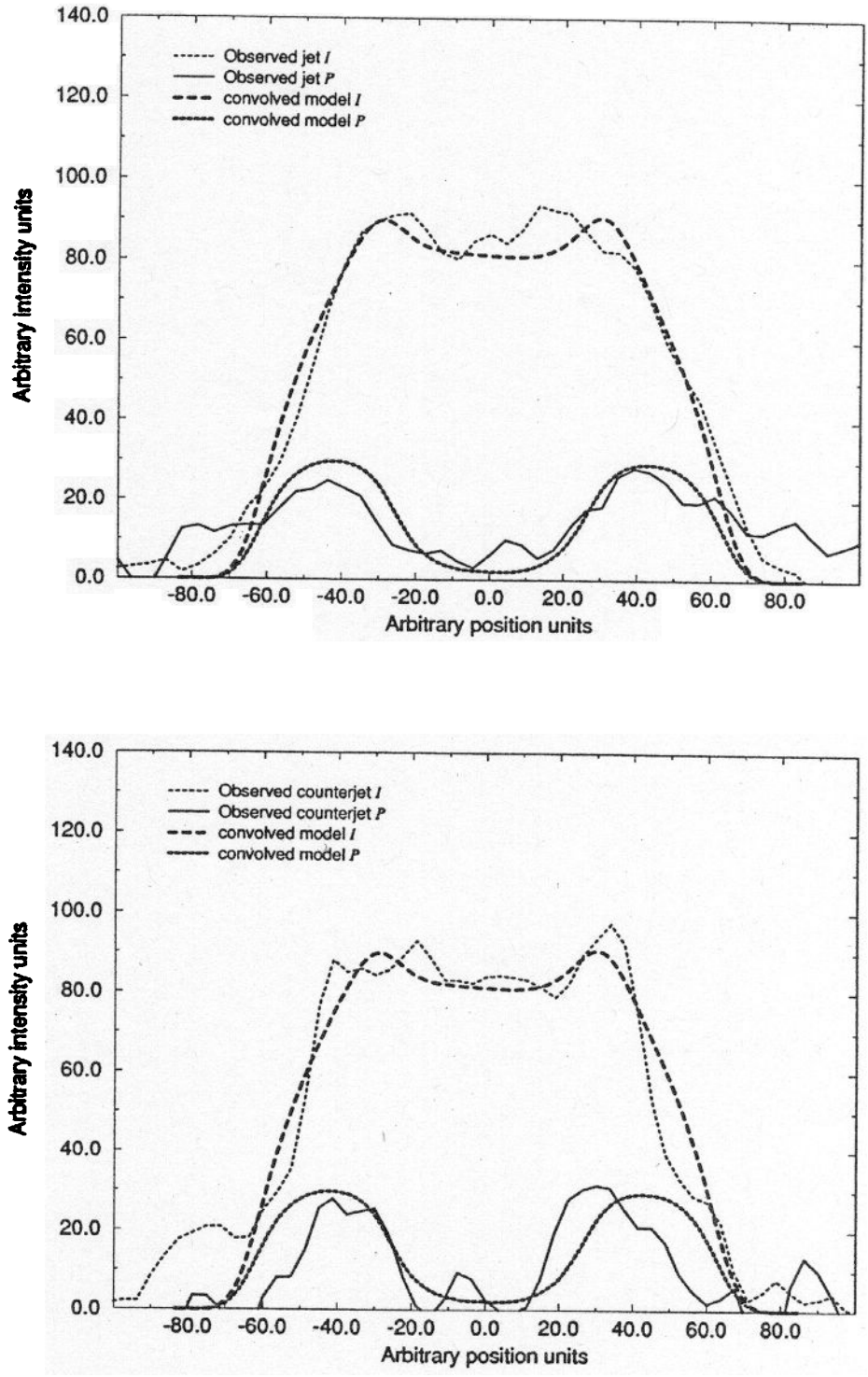

FIG. 4.—Predicted transverse I and P profiles of the model with zero emissivity in the spine, whose boundary is here at $r = 26$ (0.43 that of the jet), compared with the observed profiles. The model profiles have been convolved to the same 0".44 FWHM resolution as the observations of the jet (*upper panel*) and counterjet (*lower panel*).

RM gradient (Blandford '92)

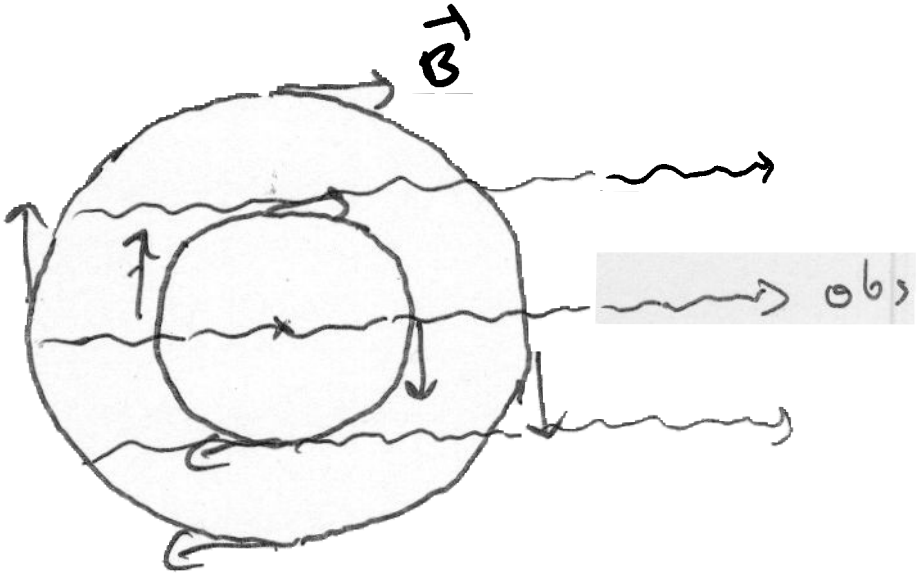

$$\Delta\chi = \lambda^2 \cdot RM$$

$$RM \propto \int n B_{\parallel} \, ds$$

$$\Delta = n_+ - n_-$$

Gabuzda et al '04
Asada et al. '02

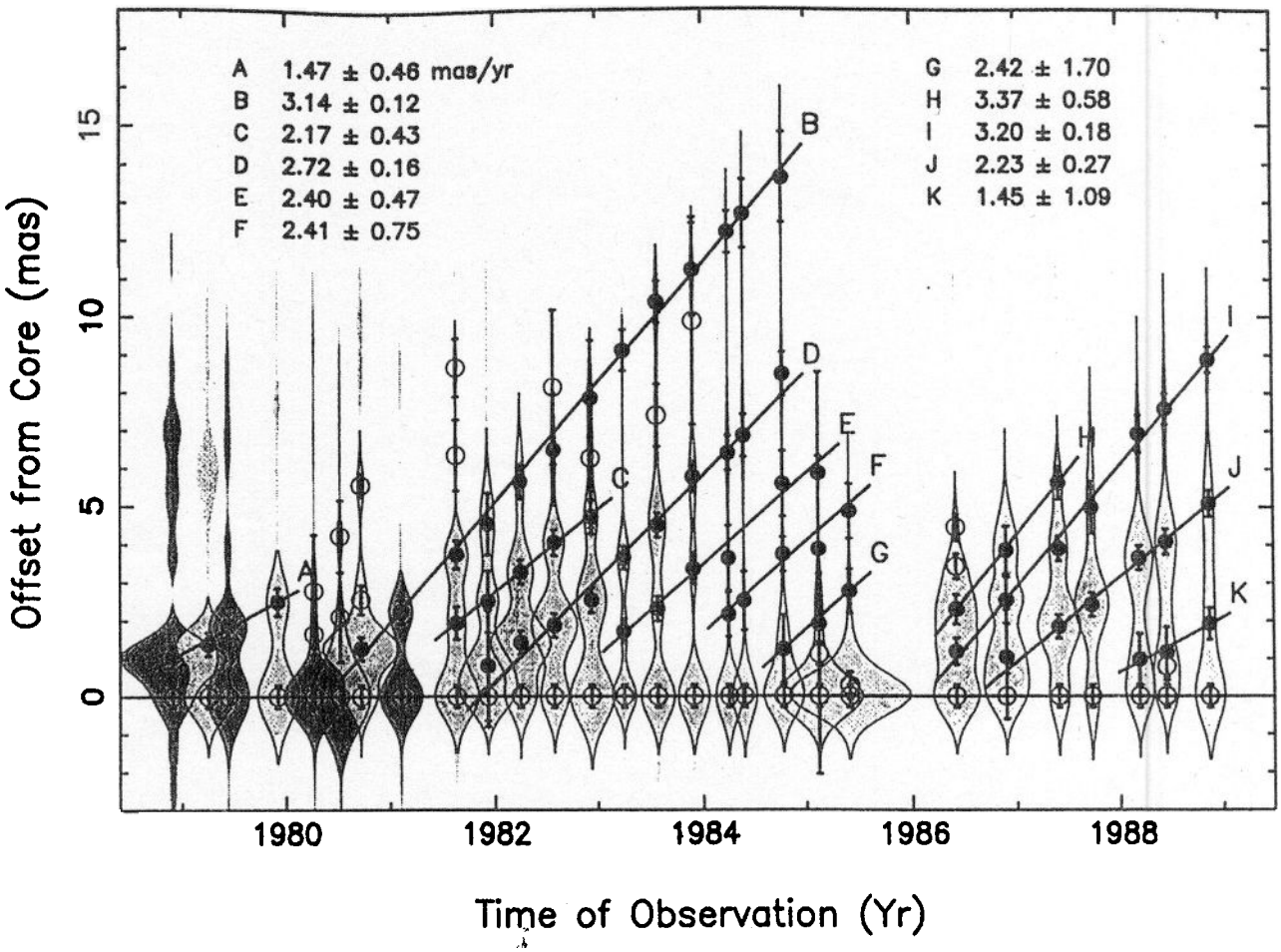

Fig. 4.— This figure shows the motions of components seen at 5 and 10.7 GHz in 3C 120 between 1978 and 1988. For each image, there is a shaded profile whose width represents the amplitude along a slice that runs along the ridge line of the jet. The 10.7 GHz images are indicated by darker shading. The thin lines that appear to outline the shading are the results of Gaussian fits to the reliable parts of the slices. The profiles have been aligned on the eastern-most feature, presumed to be the core. The fitted positions, relative to the core, of other features are shown by circles with error bars that reflect the combined formal position errors for that feature and for the core, along with an assumed alignment error. Features with filled circles are ones that are identifiable at multiple epochs and for which speeds are measured with a least squares fit. The components are labeled and a straight line with the slope corresponding to the fitted velocity is drawn through the points. The velocity for each feature, with formal errors, is written on the figure and listed in Table 4.

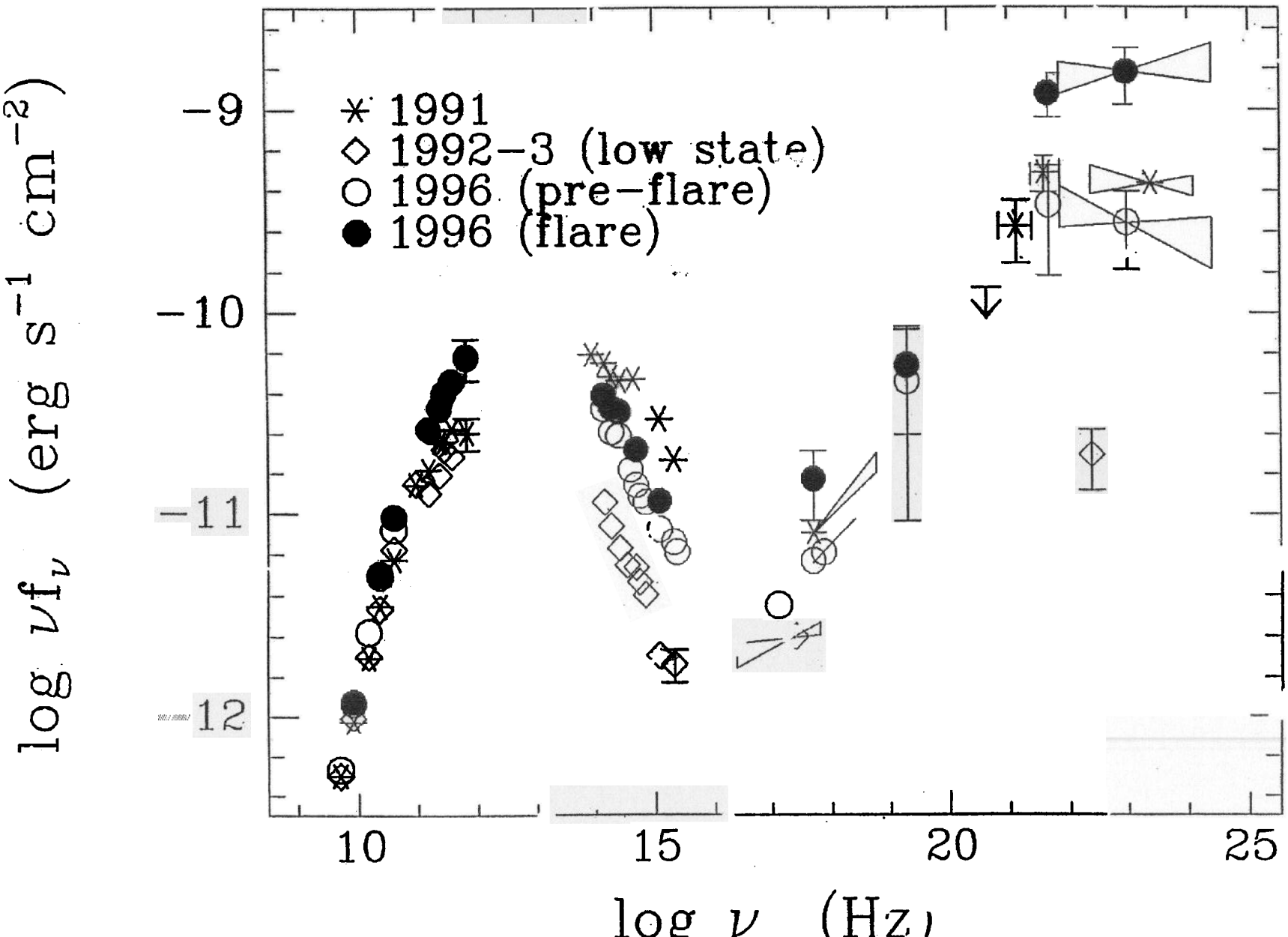
* 1991
◇ 1992–3 (low state)
○ 1996 (pre-flare)
● 1996 (flare)
−9
−10
−11
−12
10
15
20
25
log νf_ν (erg s^−1 cm^−2)
log ν (Hz)

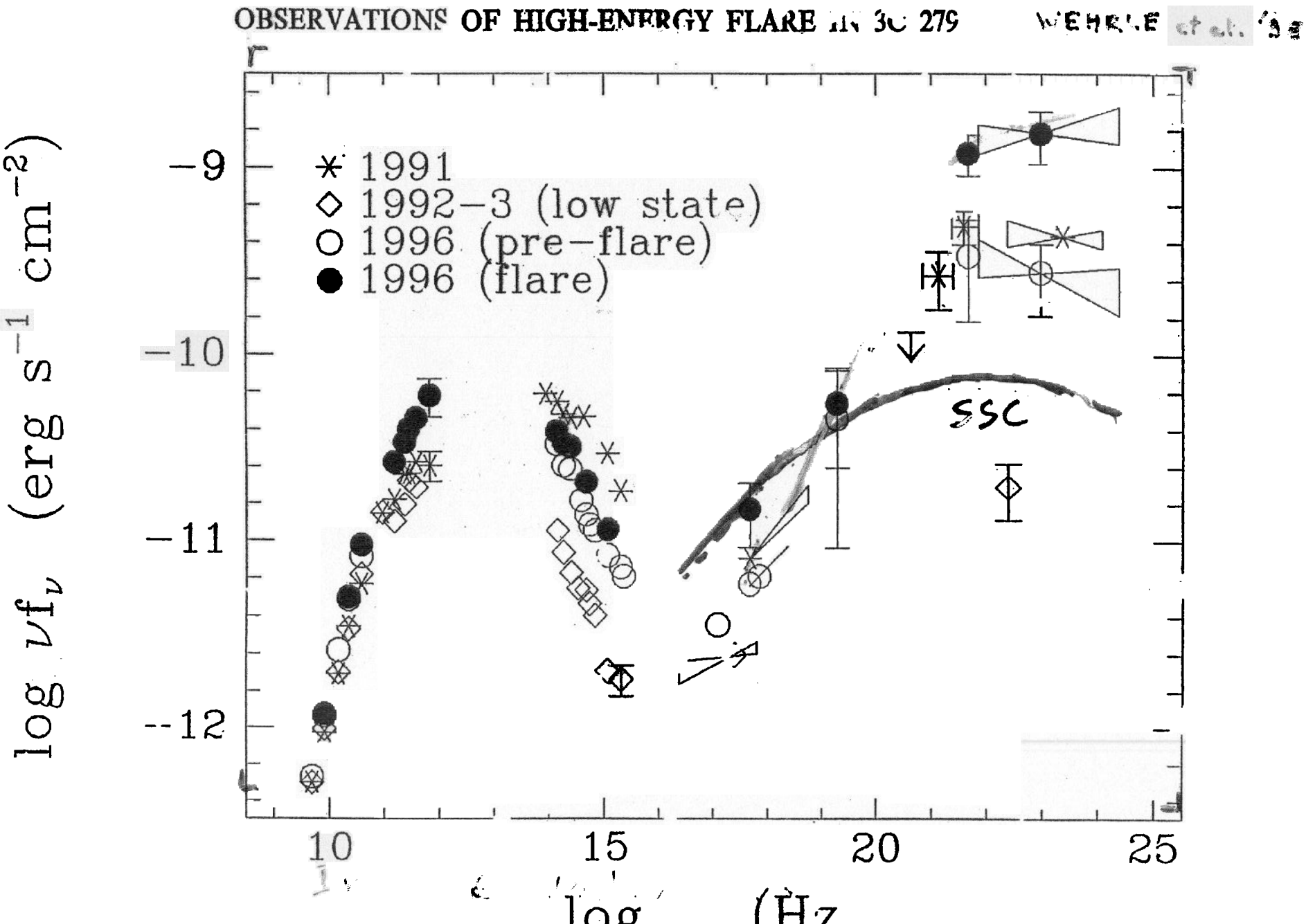
OBSERVATIONS OF HIGH-ENERGY FLARE IN 3C 279
WEHRLE et al. '98
* 1991
◇ 1992–3 (low state)
○ 1996 (pre-flare)
● 1996 (flare)
SSC
log νf_ν (erg s^-1 cm^-2)
log (Hz)
−9
−10
−11
−12
10
15
20
25

ERC

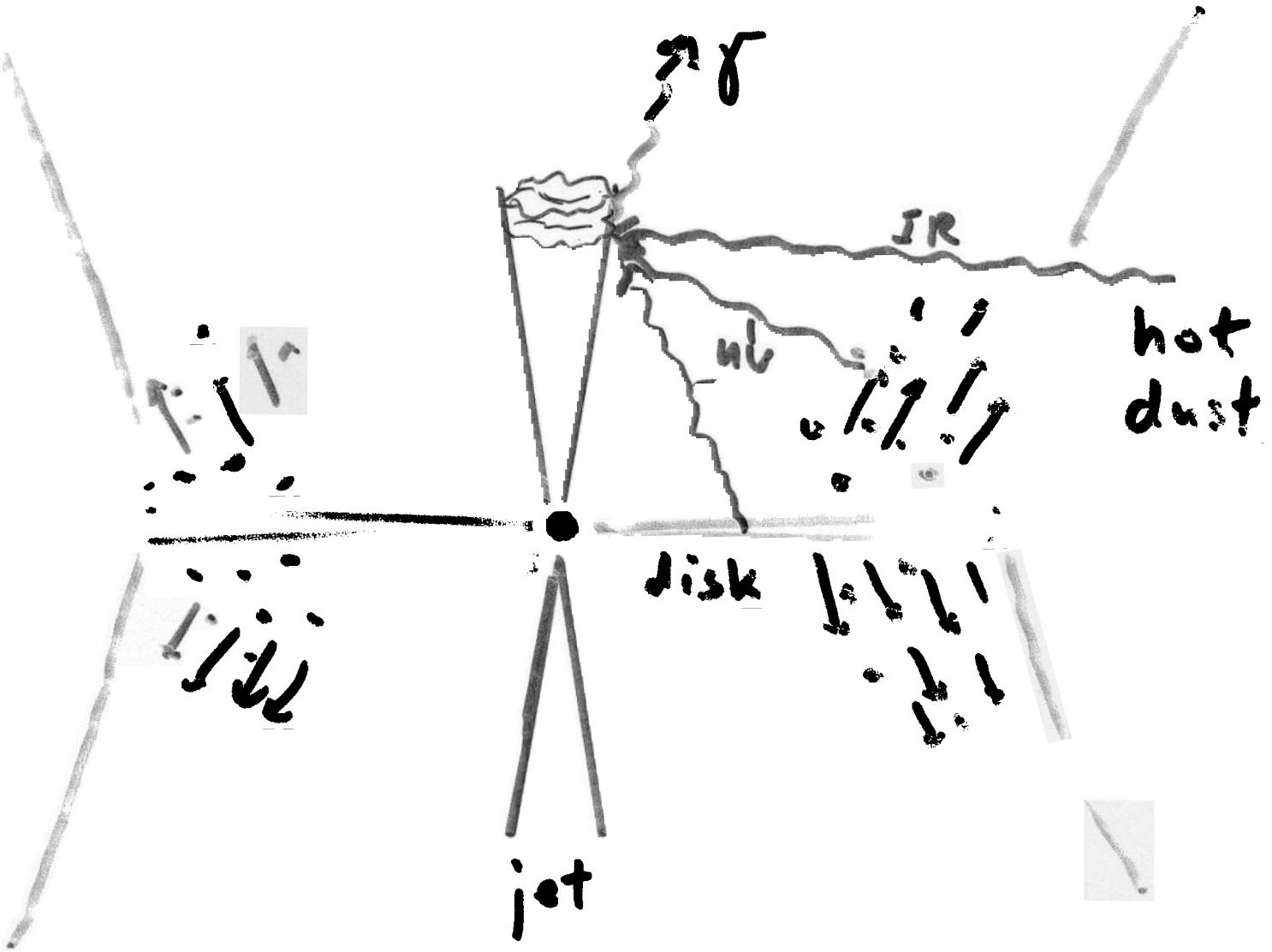

$$E = (\Gamma_j \gamma_e)^2 E_{ext}$$

Fig. 7

CITED IN TEXT | HI-RES IMAGE (166kb) |

Overall SED of 0836+710 with the spectrum calculated using the homogeneous EC model (see text). Circles are historical data taken from Kuhr et al. (1981), Wall & Peacock (1985), Impey & Tapia (1990), Wiren et al. (1992), Edelson (1994; radio), Bloom et al. (1994; far-IR), and Hartman et al. (1999; γ). Triangles are simultaneous optical data taken at the Torino Observatory. The bump in the model at $\sim 10^{15}$ Hz is due to the blackbody component used to represent the external radiation field.

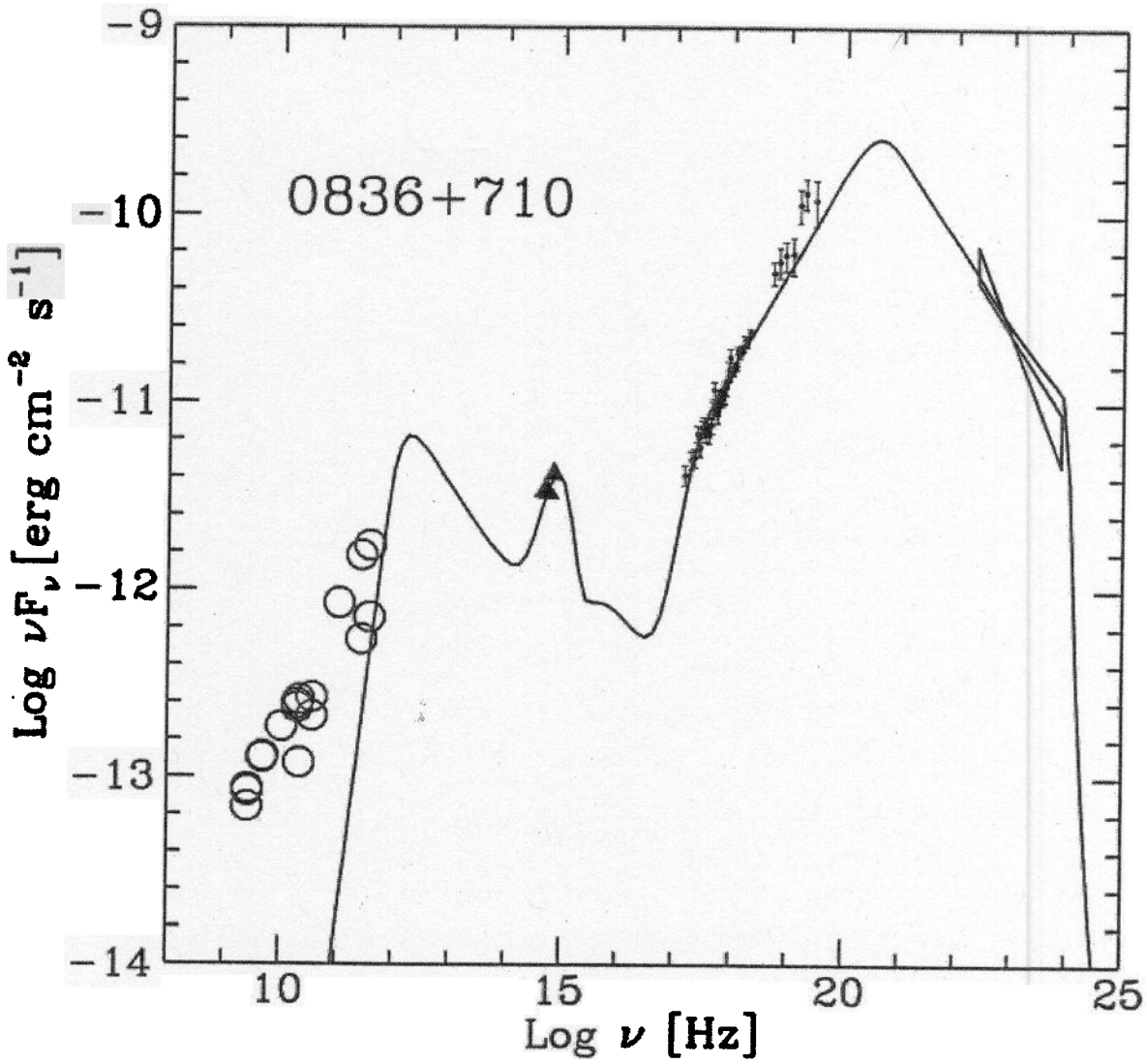

PAIRS

$$N_e = \int_1 N_\gamma \, d\gamma \quad > \quad \int_{\gamma_{min\,obs}} N_\gamma \, d\gamma$$

Radio lobes: $\sim 10^3$

Radio cores: ~ 100

Blazars:

$$\nu \sim \Gamma^2 \gamma^2 \nu_{diff} \qquad \gamma = \frac{1}{\Gamma}\left(\frac{\nu}{\nu_{diff.}}\right)^{\frac{1}{2}}$$

$h\nu_{min,obs} \sim 1\,keV$

$$h.\nu_{diff} = \begin{cases} 10\,eV \in BEL \\ 0.3\,eV \in hot\ dust \end{cases}$$

$$\Rightarrow \quad \gamma_{min,obs} \sim \begin{cases} 1 & \text{for } C(BEL) \\ 5 & \text{for } C(dust) \end{cases}$$

X-ray spectra
ERC model
} $\Rightarrow \dot{N}_e \Rightarrow L_e$

$L_e \sim 10^{45}$ erg/s $\ll L_j \sim 10^{46-47}$ erg/s

↑ radio lobes
γ-ray luminosities

⇓

Jet power dominated by protons
or magnetic fields

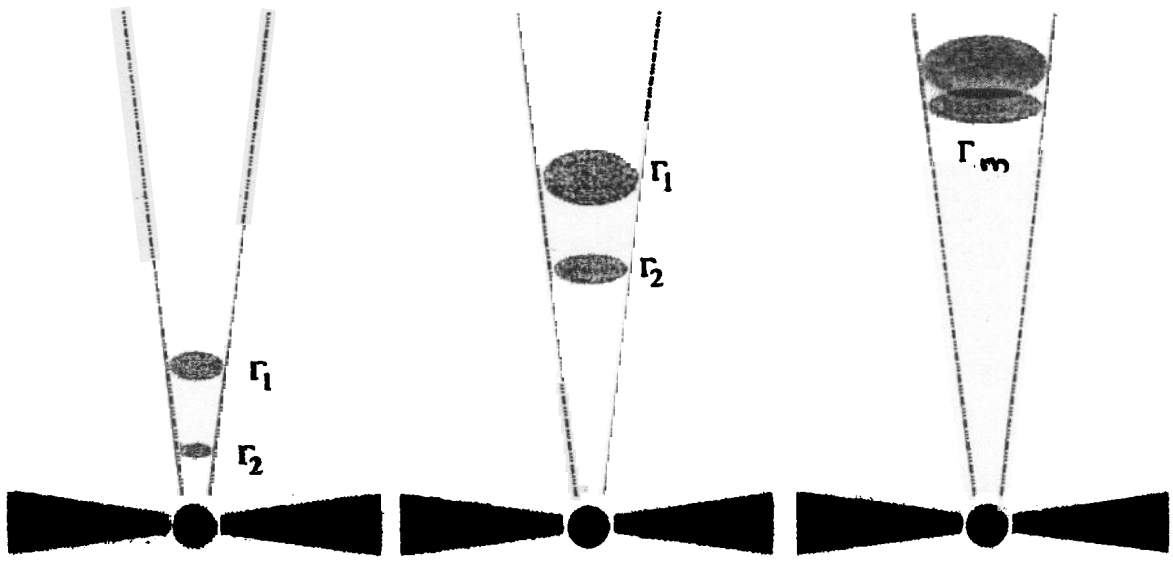

Fig. 1. Illustration of the scenario for the internal shock mechanism discussed in the text, with time progressing to the right. Two cold clouds or shells of plasma, moving with Lorentz factors Γ_1 and Γ_2 (where $\Gamma_2 > \Gamma_1$) collide, and the shocks resulting from the collision provide the site for particle acceleration.

'EXTERNAL' BULK COMPTON

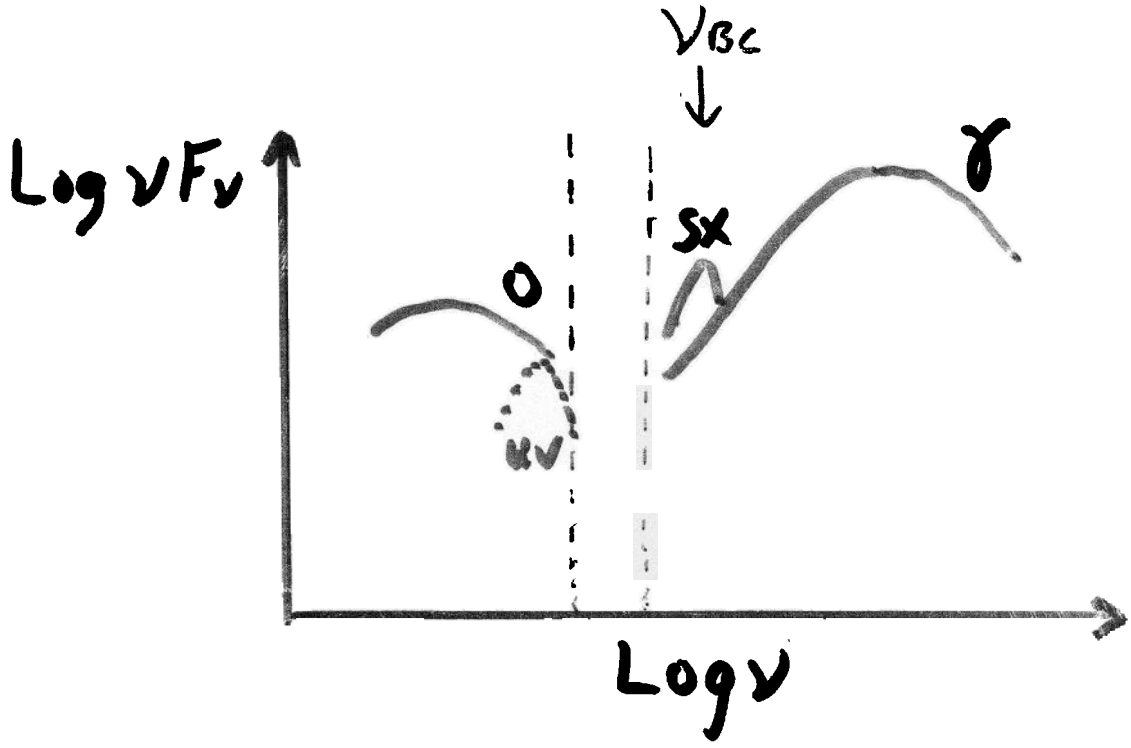

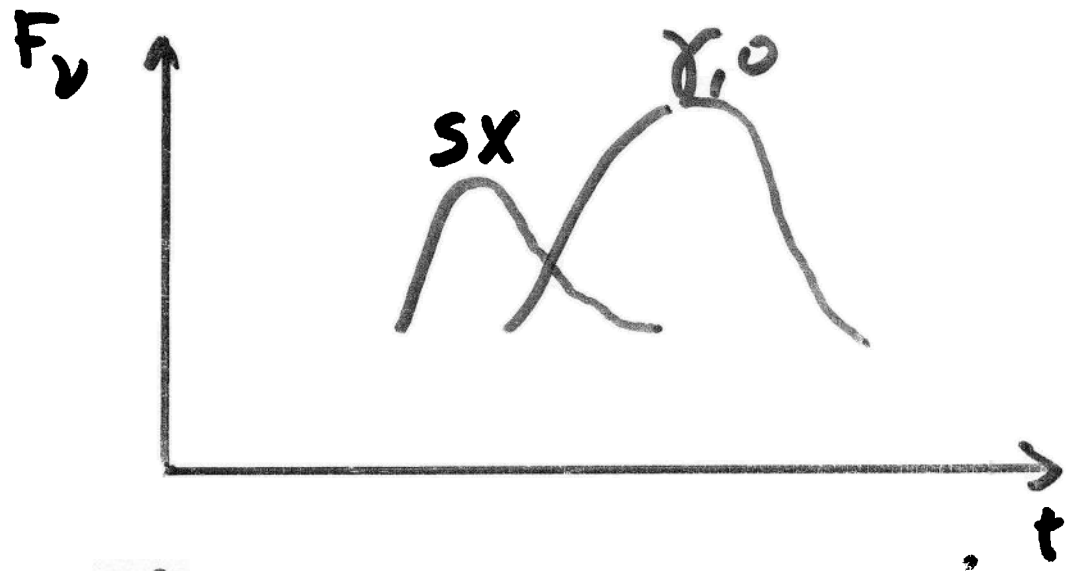

$$\nu_{BC} \sim \Gamma^2 \nu_{UV} \sim 1\ \mathrm{keV}\ [\Gamma/10]^2$$

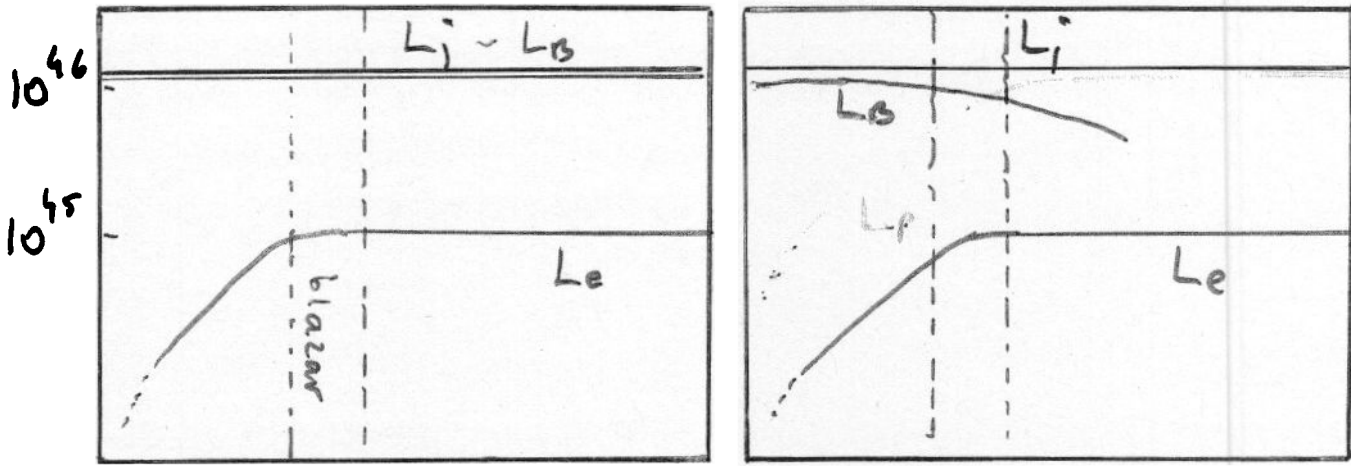

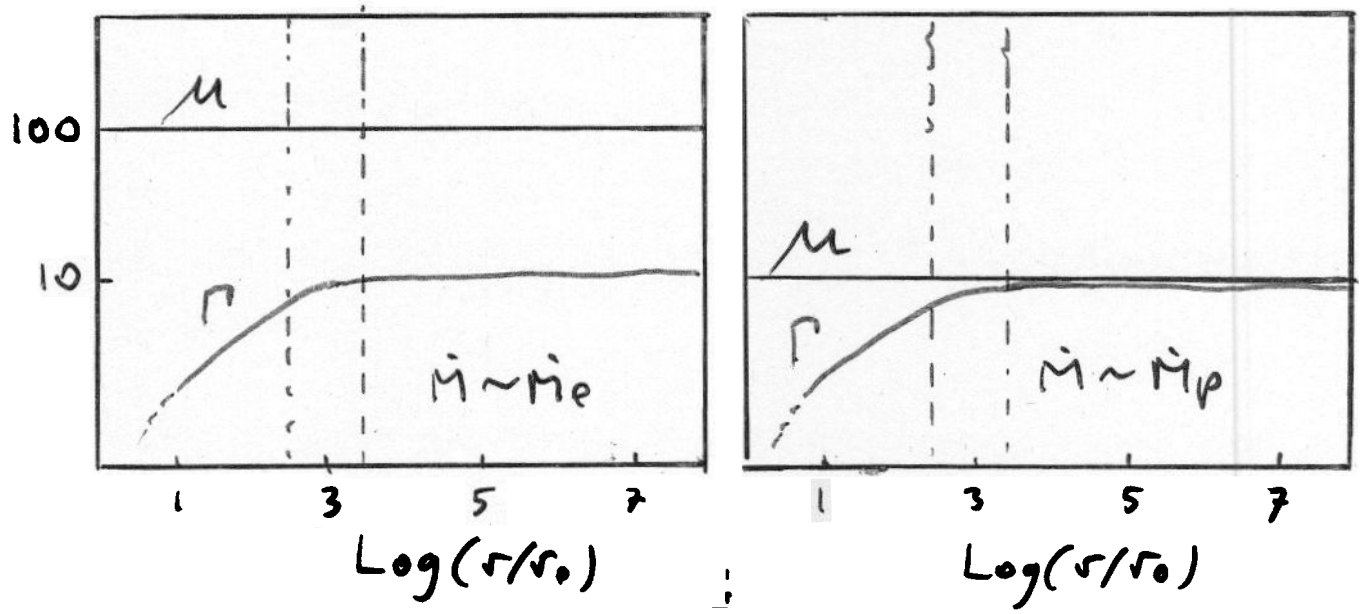

$$\mu \simeq \frac{L_j}{\dot{M}_e c^2} \sim 100$$

$$n_p \simeq 0$$

$$\sigma_\infty = 10$$

$$\mu \simeq \frac{L_j}{\dot{M}_p c^2} \sim 10$$

$$(n_e/n_p) \simeq 20$$

$$\sigma_\infty < 1$$

Are quasar jets dominated by Poynting flux?

Main conclusions:

• The kinetic energy flux of leptons, estimated from the emissivity of blazar events, is too small to support energetics of blazars and of radio lobes in quasars;

• Studies of kinematics and dynamics of quasar jets indicate that their power on the parsec- and kilo-parsec scales is likely dominated by protons, but the present data do not allow us to distinguish between the cases $\sigma \leq 1$ and $\sigma \ll 1$;

• Dynamical events associated with the blazar phenomenon and the lack of evidence for acceleration of jets beyond the blazar zone suggest that blazar activity can be related to the final stages of the conversion of initially Poynting flux dominated-jets into proton-dominated jets. MHD instabilities may play a key role in this process;

• Domination of the matter inertia by protons suggests that accretion disks have the primary role in powering quasar jets. A large pair content — deduced from the emissivity and energetics of blazar events and provided by high energy processes in the hot accretion disk corona — guarantees launching of MHD outflow even in the case of nearly vertical magnetic field lines.